Supporting Information

Quinoxalinedione deprotonation is important for glutamate receptor binding

Adela Dudić and Andreas Reiner #

Department of Biology and Biotechnology, Ruhr University Bochum, Bochum, Germany

Supporting Information

1. ¹ H-NMR measurements and determination of extinction coefficients	p. 2
2. Fluorescence emission spectra of the GluA2 LBD in the absence and presence of DNQX and CNQX	p. 3
3. Fluorescence measurements in the presence of high quinoxalinedione concentrations (inner filter effect)	p. 5
4. Analysis of titration and competition experiments	p. 6
5. Absorbance measurements and determination of pK_a values	p. 7
6. Coupling formalism and estimation of K_d^0 and K_d^-	p. 10
Supporting references	p. 11
Table S1. Summary of pK_a values and absorbance properties	p. 12
Table S2 . Summary of ligand binding and competition assays	p. 13

1. ¹H-NMR measurements and determination of extinction coefficients

In order to determine precise molar extinction coefficients for DNQX and CNQX, we relied on a NMR-based approach. We added L-tryptophan (Trp), for which the molar extinction coefficient is known ($\epsilon_{280 \text{ nm}} = 5600 \text{ M}^{-1} \text{ cm}^{-1}$ (Schmid, 1997)), as an internal concentration standard for comparing the integrals of selected ¹H resonances. Solutions of DNQX (10 mM), CNQX (10 mM), and Trp (20 mM, Sigma, 93659) were prepared in distilled water, and in a separate set of experiments in DMSO- d_6 . ¹H spectra were obtained using 1D zg30 (DMSO- d_6) and 1D zgcptqpr (H₂O) sequences on a 300 MHz Avance III 300 spectrometer (Bruker) and were analyzed using MestReNova 12 (Mestrelab Research). The integrals of the different protons within CNQX and Trp closely matched the expectations.

We then compared the integrals of all aromatic proton resonances of DNQX or CNQX with our standard, Trp. The ratios of the corresponding integrals were similar between the different samples. We used these signal ratios in combination with the absorbance measurements of the stock solutions diluted into 50 mM NaCl, 20 mM HEPES, pH 7.0 to calculate the extinction coefficients (see Table S1). The concentration of the Trp stock solutions closely matched the expectations from our weight measurements, whereas the DNQX and CNQX concentrations were found to be ~23 % and ~21 % lower than estimated based on weight.

6,7-Dinitroquinoxaline-2,3(1*H***,4***H***)-dione** (DNQX): ¹**H NMR** (DMSO- d_6 with 0.03% v/v TMS, 300 MHz): δ 7.51 ppm (s, 2H). **Absorption** (50 mM NaCl, 20 mM HEPES, pH 7.0): $\epsilon_{280 \text{ nm}} = 18887 \text{ M}^{-1} \text{ cm}^{-1}$.

6-Cyano-7-nitroquinoxaline-2,3(1*H***,4***H***)-dione** (CNQX): ¹**H NMR** (DMSO- d_6 with 0.03% v/v TMS, 300 MHz): δ 7.83 ppm (s, 1H), 7.32 ppm (s, 1H). **Absorption** (50 mM NaCl, 20 mM HEPES, pH 7.0): $\epsilon_{280 \text{ nm}} = 26643 \text{ M}^{-1} \text{ cm}^{-1}$.

2. Fluorescence emission spectra of the GluA2 LBD in the absence and presence of DNQX and CNQX

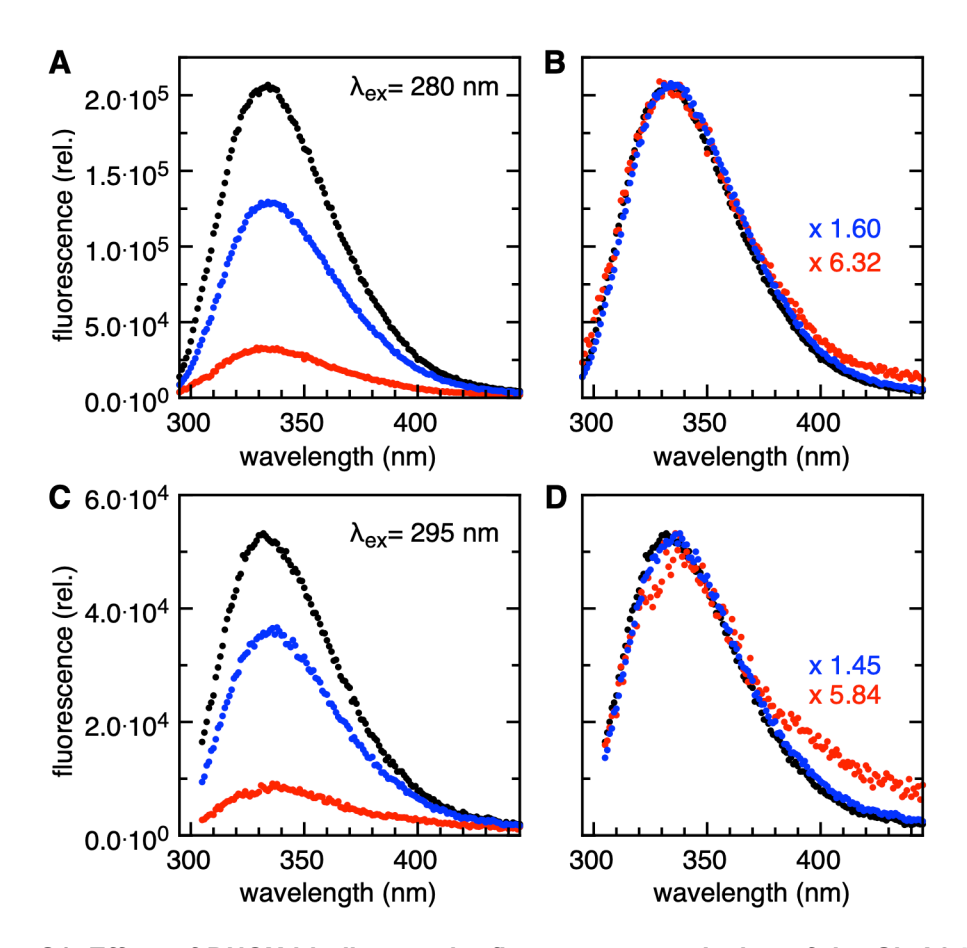


Figure S1. Effect of DNQX binding on the fluorescence emission of the GluA2 LBD. Spectra obtained with 0.5 μ M GluA2 LBD in the absence of ligand (black), after addition of 1 μ M DNQX (red), and after subsequent addition of 60 μ M glutamate (blue). (A) Fluorescence emission spectra upon excitation at 280 nm. (B) Normalized emission spectra from (A) with normalization factors as indicated. (C) Fluorescence emission spectra upon excitation at 295 nm. (D) Normalized emission spectra from (C). Measurements were performed in 50 mM NaCl, 20 mM HEPES, pH 7.0. The excitation slit width was 2 nm and the emission slit width 2 nm (1 nm increment).

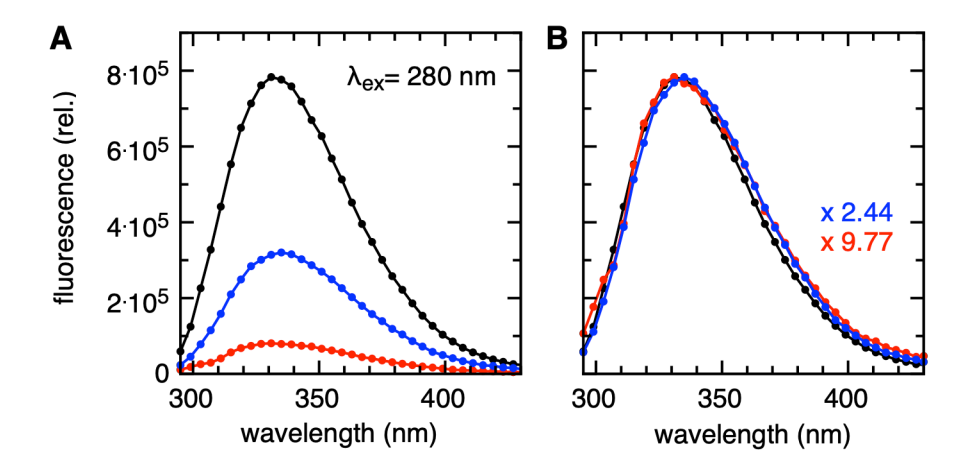


Figure S2. Fluorescence decrease of the GluA2 LBD upon CNQX binding and partial fluorescence recovery upon glutamate addition. (A) Fluorescence emission spectra obtained with 0.5 μ M GluA2 LBD in the absence of ligand (black), after addition of 6.17 μ M CNQX (red), and after subsequent addition of 160 μ M glutamate (blue) upon excitation at 280 nm. The fluorescence recovery is already reduced due to the inner filter effect of CNQX. (B) Normalized emission spectra from (A) with normalization factors as indicated. Measurements were performed in 50 mM NaCl, 20 mM HEPES, pH 6.0. The excitation slit width was 2 nm, the emission slit width 4 nm (4 nm increment).

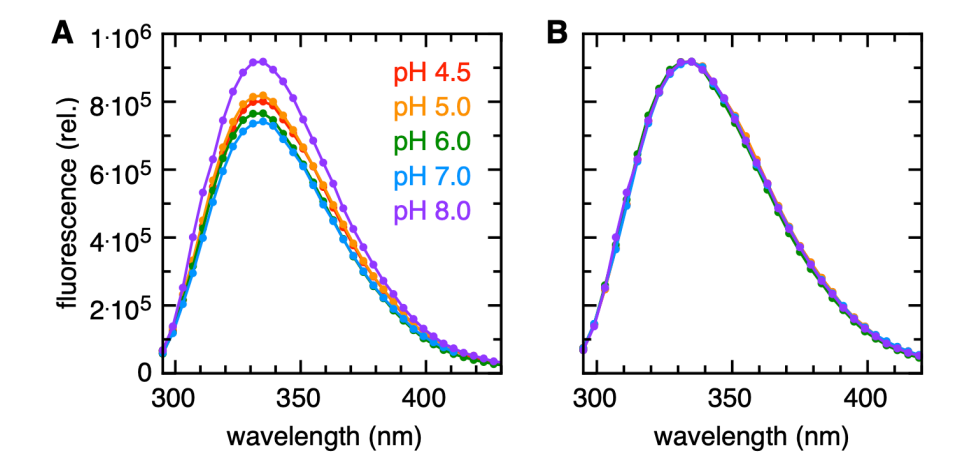


Figure S3. Fluorescence of the apo-GluA2 LBD at different pH values. (A) Fluorescence emission spectra at indicated pH values, corrected for differences in concentration (0.5 μM LBD for pH 4.5-6.0; 0.2 μM LBD for pH 7.0 and pH 8.0) upon excitation at 280 nm. The fluorescence emissions were recorded on different days but show no systematic variation with pH (average fluorescence intensity $(8.1 \pm 0.6) \cdot 10^5$ units (mean \pm SD)). **(B)** Normalized emission spectra from (A). Measurements were performed in 50 mM NaCl, 20 mM HEPES. The excitation slit width was 2 nm, the emission slit width 4 nm (4 nm increment).

3. Fluorescence measurements in the presence of high quinoxalinedione concentrations (inner filter effect)

Quinoxalinediones show a strong absorbance that overlaps with the excitation and emission of Trp (Fig. S5-8). To assess the contribution of inner filter effects (Lakowicz, 2006) to our fluorescence measurements, we performed measurements using N-acetyl-L-tryptophanamide (Sigma, A6501) as a reference compound and added increasing concentrations of DNQX (Fig. S4). Indeed, at [DNQX] \geq 3 μ M we observed a fluorescence decrease, which was neither explained by the modest volume increase (1 % per addition) nor photo-bleaching (< 0.3 %). The decrease of the fluorescence signal with increasing quinoxalinedione concentration, F([QX]), was well described as a single exponential decrease with the quenching constant K_{IF} (Eq. S1):

$$F([QX]) = F_0 e^{-[QX]/K_{IF}}$$
 (Eq. S1)

Using non-linear least-square fitting we obtained $K_{\rm IF} = (33.5 \pm 1.0) \, \mu \rm M$, which we used for analyzing all our data. Since $K_{\rm IF}$ also depends on the spectrometer settings and sample/beam geometry, it will have to be determined for each experimental setup. The extinction at the relevant wavelengths differs only slightly for the different pH values (Fig. S5), which makes this calibration useful for all pH values. Collisional quenching or FRET to unbound quinoxalinedione should not contribute in this concentration range.

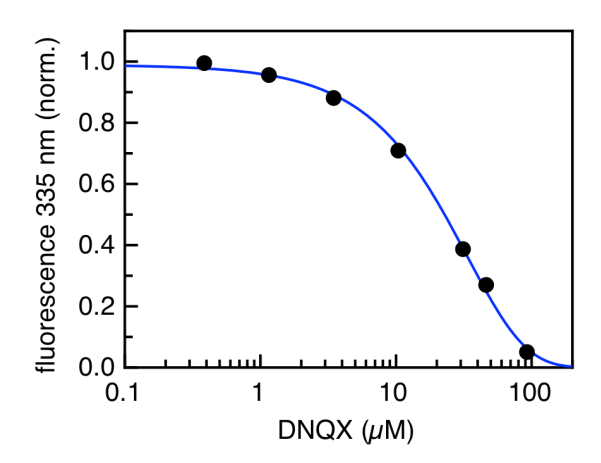


Figure S4. Trp fluorescence in the presence of high DNQX concentrations. DNQX was added to 2 μ M *N*-acetyl-L-tryptophanamide (NATA) in 50 mM NaCl, 20 mM HEPES, pH 6.0. The plotted values are corrected for the volume change (1 % per addition) and a fit with Eq. S1 yielded $K_{\rm IF}$ = (33.5 ± 1.0) μ M and F_0 = 0.99 ± 0.01 (blue line). The fluorescence excitation was 280 nm (2 nm slit width), the emission slit width 4 nm.

4. Analysis of titration and competition experiments

To analyze binding/unbinding of a single ligand (Eq. 2a) we used the general solution without any approximations, which is a quadratic equation (Eq. 2bc). The results obtained for the titration experiments are shown in Fig. 2B and Fig. 3A,C and are summarized in Table S2.

Our competition experiments, i.e. glutamate binding in the presence of a quinoxalinedione ligand (Fig. 2C and Fig. 3B), are characterized by the simultaneous presence of two ligand types, A and B, which compete for the same receptor binding site, R:

$$RA + B \rightleftharpoons R + A + B \leftrightharpoons RB + A$$
 (Eq. S2a)

Also in this case we resorted to the general solution, since none of the binding partners was in large excess. The cubic solution to this problem is given by Wang (Wang, 1995) using the expressions:

$$a = K_d^A + K_d^B + [A]_0 + [B]_0 - [R]_0$$
 (Eq. S2b)

$$b = K_d^B \cdot ([A]_0 - [R]_0) + K_d^A \cdot ([B]_0 - [R]_0) + K_d^A \cdot K_d^B$$
 (Eq. S2c)

$$c = -K_d^A \cdot K_d^B \cdot [R]_0$$
 (Eq. S2d)

$$\theta = arc \cos \frac{-2a^3 + 9ab - 27c}{2 \cdot (a^2 - 3b)^{3/2}}$$
 (Eq. S2e)

The concentrations [RA] and [RB] are then given by:

$$[RA] = \frac{[A]_0 \cdot \{2\sqrt{(a^2 - 3b)}\cos(\theta/3) - a\}}{3 \cdot K_d^A + \{2\sqrt{(a^2 - 3b)}\cos(\theta/3) - a\}}$$
(Eq. S2f)

[RB] =
$$\frac{[B]_0 \cdot \{2\sqrt{(a^2 - 3b)\cos(\theta/3) - a}\}}{3 \cdot K_d^B + \{2\sqrt{(a^2 - 3b)\cos(\theta/3) - a}\}}$$
 (Eq. S2g)

The measured fluorescence signal is then:

$$\frac{F([B]_0, [A]_0)}{F_R} = \left(\frac{[RA]}{[R]_0} \cdot f_{RA} + \frac{[RB]}{[R]_0} \cdot f_{RB} + \frac{[R]_0 - [RA] - [RB]}{[R]_0}\right) \cdot e^{-[B]_0 / K_{IF}} \quad (Eq. S2h)$$

where $f_{RA} = F_{RA}/F_R$ denotes the relative fluorescence intensity of the ligand A bound receptor, and $f_{RB} = F_{RB}/F_R$ of the ligand B bound receptor, compared to the apo-LBD. The inner filter effect of ligand B is taken into account according to Eq. S1.

5. Absorbance measurements and determination of pK_a values

Absorbance measurements of DNQX, CNQX, NBQX and YM90K were performed as described in Material and methods. To determine the pK_a values and to confirm the respective model, we selected different wavelengths, which encompassed both isosbestic points as well as absorbance maxima, for global analysis (Fig. S5-8).

DNQX and **CNQX** showed diprotic behavior (Eq. 4 (de Levie, 1993), Fig. S5 and Fig. S6), whereas NBQX and YM90K show additional deprotonation steps. The simplest model that described the changes observed for **NBQX** (Fig. S7) was a simple triprotic acid (Eq. S3a-b). In this case, one of the transitions can be attributed to the deprotonation of the sulfonamide group, similar to benzenesulfonamide, which has a p $K_a \sim 10$ (Cotton and Stokely, 1970).

$$AH_3 \leftrightharpoons AH_2 + H \leftrightharpoons AH + 2H \leftrightharpoons A + 3H$$
 (Eq. S3a)

$$A(pH) = \frac{1}{10^{-3 pH} + 10^{-2 pH - pK_a^1} + 10^{-pH - pK_a^1 - pK_a^2} + 10^{-pK_a^1 - pK_a^2 - pK_a^3}} \cdot \left(\frac{A_{AH3}}{10^{3 pH}} + \frac{A_{AH2}}{10^{2 pH + pK_a^1}} + \frac{A_{AH}}{10^{pH + pK_a^1 + pK_a^2}} + \frac{A_A}{10^{pK_a^1 + pK_a^2 + pK_a^3}}\right)$$
(Eq. S3b)

For **YM90K** we also expected a triprotic behavior due to the presence of an imidazole group. However, while many wavelengths show rel. broad transitions, a fourth transition is clearly present at some wavelengths, e.g. at 301 nm (Fig. S8). This indicates that two of the deprotonations, probably from the imidazolium cation to imidazole and from the neutral quinoxalinedione to the quinoxalinedione monoanion, occur with similar pK_a values. This would give rise to parallel deprotonation pathways and intermediates with different spectroscopic properties. This notion is supported by the pK_a values reported by (Ohmori, et al., 1994).

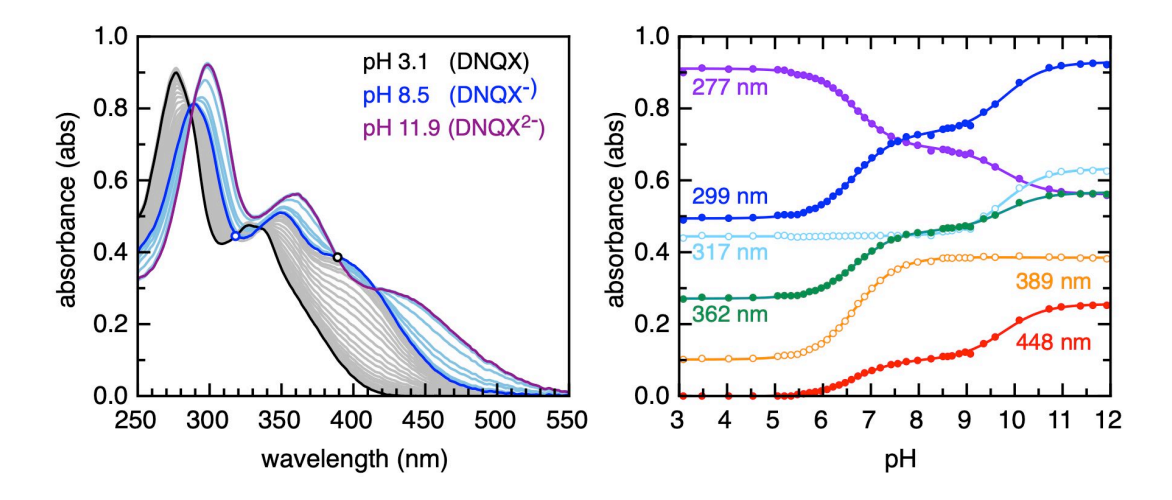


Figure S5. Absorbance measurements and determination of pK_a values of DNQX. (A) Absorbance spectra of 38 µM DNQX measured in the range of pH 3-12. The spectra show two separate sets of isosbestic points and are consistent with the existence of three differently absorbing species, which we attribute to DNQX (black), DNQX⁻ (blue) and DNQX²⁻ (purple). (B) Absorbance changes (points) at different wavelengths were selected for analysis. A global fit of this data with Eq. 4 (lines) yields $pK_a^1 = 6.68 \pm 0.01$ and $pK_a^2 = 9.77 \pm 0.01$, respectively.

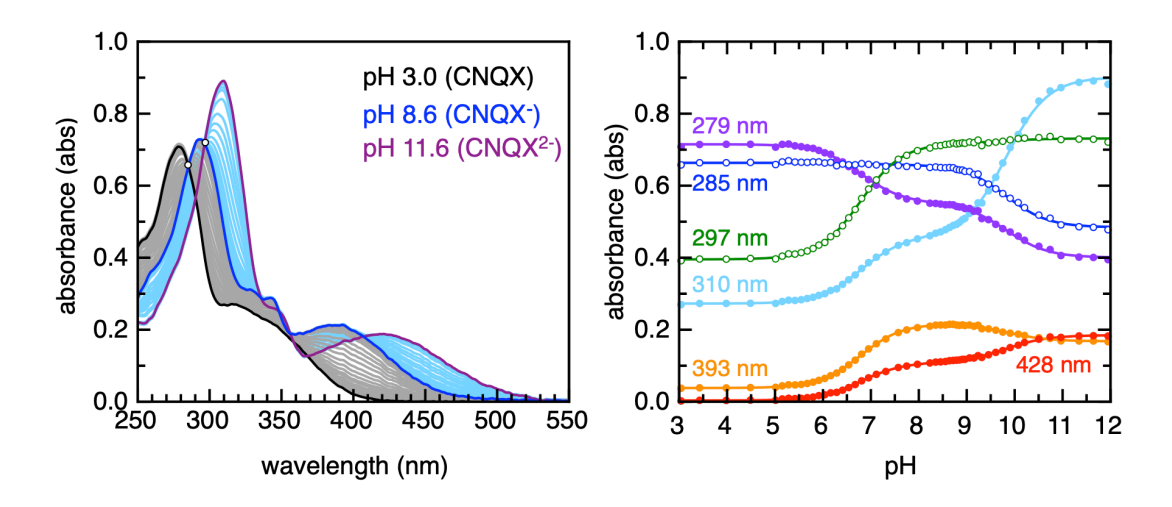


Figure S6. Absorbance measurements and determination of p K_a values of CNQX. (A) Absorbance spectra of 23.7 μM CNQX measured in the range of pH 3-12. The spectra show two separate sets of isosbestic points and are consistent with the existence of three differently absorbing species, which we attribute to CNQX (black), CNQX⁻ (blue) and CNQX²⁻ (purple). (B) Absorbance changes (points) at different wavelengths were selected for analysis. A global fit of this data with Eq. 4 (lines) yields p $K_a^1 = 6.78 \pm 0.01$ and p $K_a^2 = 9.82 \pm 0.01$, respectively.

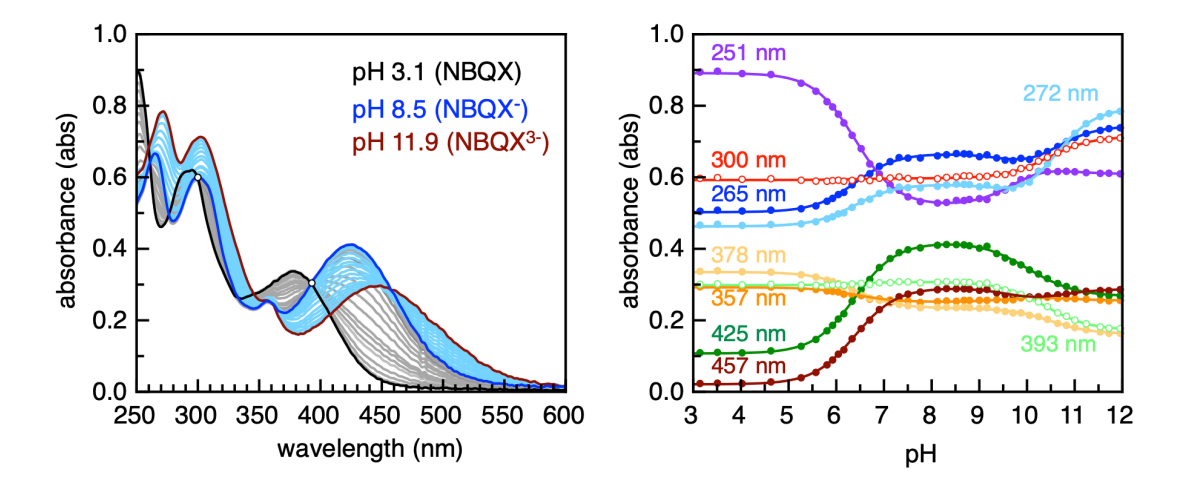


Figure S7. Absorbance measurements and determination of p K_a values of NBQX. (**A**) Absorbance spectra of ~50 μM NBQX measured in the range of pH 3-12. The spectra are consistent with the existence of four differently absorbing species, which we attribute to NBQX (black), NBQX⁻ (blue), NBQX²⁻ (not separable) and NBQX³⁻ (dark red). (**B**) Absorbance changes (points) at different wavelengths were selected for analysis. A global fit of this data with Eq. S3ab (lines) yields p K_a^1 = 6.39 ± 0.01, p K_a^2 = 9.73 ± 0.03 and p K_a^3 = 10.57 ± 0.02, respectively.

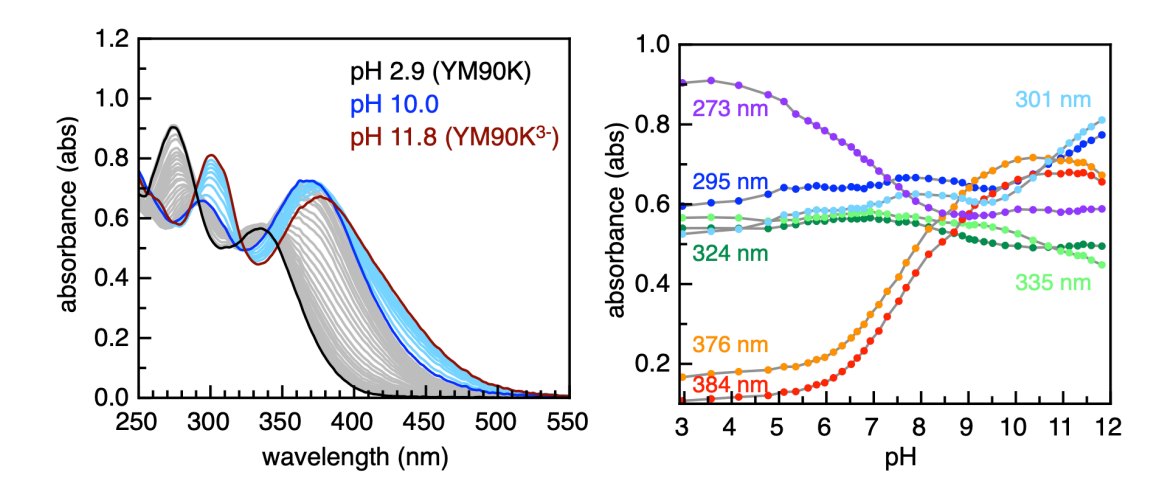


Figure S8. Absorbance measurements of YM90K. (A) Absorbance spectra of ~50 μ M YM90K measured in the range of pH 3-12. (B) Absorbance changes (points) at selected wavelengths are consistent with the existence of up to five differently absorbing species and p K_a values in the range of 4-11. For details see text SI.

6. Coupling formalism and estimation of K_d^0 and K_{d^-}

Binding/unbinding of a ligand that undergoes protonation/deprotonation represents a four-state scheme (Fig. 5A and below), in which the binding and deprotonation equilbria are thermodynamically coupled. This formalism is readily applicable to quinoxalinedione binding at GluA2 LBDs assuming that the affinity changes in the tested pH range reflect only the first deprotonation and that all changes can be attributed to the changes in the protonation of the ligand, but not the LBD (we found that glutamate binding does not change in this pH range).

The apparent dissociation constant, $K_{d,obs}$ is then given by:

$$K_{d,obs}(pH) = \frac{[R] \cdot [L^{-}] + [R] \cdot [LH]}{[RL^{-}] + [RLH]} = \frac{[R] [L^{-}] \cdot \left(1 + \frac{LH}{[L^{-}]}\right)}{[RL^{-}] \cdot \left(1 + \frac{[RLH]}{[RL^{-}]}\right)} =$$

$$= K_{d}^{-} \cdot \frac{1 + 10^{pK_{a}^{free} - pH}}{1 + 10^{pK_{a}^{bound} - pH}}$$
(Eq. S4a)

In addition, microscopic reversibility gives:

$$K_{\rm d}^{0} \cdot 10^{\,\rm pH - p} K_{\rm a}^{\rm free} = K_{\rm d}^{-} \cdot 10^{\,\rm pH - p} K_{\rm a}^{\rm bound}$$
or:
$$10^{\,\rm p} K_{\rm a}^{\rm bound - pH} = K_{\rm d}^{-} / K_{\rm d}^{0} \cdot 10^{\,\rm p} K_{\rm a}^{\rm free - pH}$$
(Eq. S4b)

The combination of Eq. S4a with Eq. S4b yields:

$$K_{\rm d}(\rm pH) = \frac{K_{\rm d}^{-} \cdot K_{\rm d}^{0} \cdot (10^{\rm pH} + 10^{\rm pK_{\rm a}^{\rm free}})}{K_{\rm d}^{0} \cdot 10^{\rm pH} + K_{\rm d}^{-} \cdot 10^{\rm pK_{\rm a}^{\rm free}}})$$
(Eq. 1)

Supporting references

Cotton, F.A., and Stokely, P.F. (1970). Structural basis for the acidity of sulfonamides. Crystal structures of dibenzensulfonamide and its sodium salt. J. Am. Chem. Soc. *92*, 294-302.

De Levie, R. (1993). Explicit expressions of the general form of the titration curve in terms of concentration. J. Chem. Educ. 70, 209-217.

Lakowicz, J.R. (2006). Principles of fluorescence spectroscopy, Third edition (New York, USA: Springer)

Ohmori, J., Sakamoto, S., Kubota, H., Shimizu-Sasamata, M., Okada, M., Kawasaki, S., Hidaka, K., Togami, J., Furuya, T., and Murase, K. (1994). 6-(1H-imidazol-1-yl)-7-nitro-2,3(1*H*,4*H*)-quinoxalinedione hydrochloride (YM90K) and related compounds: Structure-activity relationships for the AMPA-type non-NMDA receptor. J. Med. Chem. *37*, 467-475.

Schmid, F.X. (1997). Optical spectroscopy to characterize protein conformation and conformational changes. In Protein Structure: A practical approach, T.E. Creighton, ed. (Oxford: IRL Press), pp. 261-297.

Wang, Z.X. (1995). An exact mathematical expression for describing competitive binding of two different ligands to a protein molecule. FEBS Lett. *360*, 111-114.

Table S1. Summai	ry of p K_a values a	and absorbance	properties	
	DNQX	CNQX	NBQX	YM90K
pK _a values ^a	6.68, 9.77	6.78, 9.82	6.39, 9.73, 10.57	4.7, 7.4, 10.8 ^d
ε _{280 nm} (M ⁻¹ cm ⁻¹), pH 7.0 ^b	18887	26643	n.d.	n.d.
wavelengths (rel.	intensity ^c)			
QX maxima	277 nm (1.15) 327 nm (0.61)	279 nm (1.15) 315 nm (0.44)	251 nm (1.84) 295 nm (1.28) 378 nm (0.69)	273 nm (1.26) 335 nm (0.79)
QX/QX ⁻ isosbestic points	287 nm (1.00) 317 nm (0.57) 335 nm (0.60)	285 nm (1.06)	261 nm (1.32) 278 nm (1.06) 300 nm (1.23) 333 nm (0.54) 393 nm (0.63)	n.d.
QX ⁻ maxima	289 nm (1.04) 349 nm (0.65) 396 nm (0.48)	293 nm (1.18) 328 nm (0.50) 342 nm (0.47) 393 nm (0.34)	265 nm (1.37) 300 nm (1.24) 357 nm (0.52) 425 nm (0.85)	n.d.
QX ⁻ /QX ²⁻ isosbestic points	289 nm (1.04) 389 nm (0.50) 415 nm (0.38)	297 nm (1.15) 336 nm (0.46) 348 nm (0.41) 357 nm (0.30) 407 nm (0.29)	n.d.	n.d.
QX ²⁻ maxima	299 nm (1.18) 362 nm (0.72) 448 nm (0.32)	310 nm (1.44) 347 nm (0.41) 428 nm (0.30)	n.d.	n.d.
QX ⁻ /QX ³⁻ isosbestic points	-	-	357 nm (0.52) 457 nm (0.05)	n.d.
QX ³⁻ maxima	-	-	272 nm (1.61) 302 nm (1.47) 356 nm (0.53) 449 nm (0.61)	301 nm (1.13) ° 376 nm (0.94) °

Summary of the absorbance data shown in Fig. 4 and Fig. S5-8.

^a pK_a values were obtained by global fitting of the absorbance data, for details see Fig. S5-7.

^b Molar extinction coefficients were determined with support from ¹H-NMR measurements.

^c Relative absorbance compared to the absorbance at pH 7.0 and 280 nm.

^d Ohmori et al., 1994.

e Data at pH 11.8.

Table S2. Summary of ligand binding and competition assays

Direct binding assays	ng assays						
DNQX	[LBD] (µM)	K _d DNQX (µM) ^a	A ^{DNQX·LBD} (rel.) ^b	CNQX	[LBD] (µM)	K _d CNQX (µM) ^a	A ^{CNQX·LBD} (rel.) ^b
pH 4.5	0.5	3.60 ± 0.54	0.23 ± 0.01				
pH 5.0	0.5	0.99 ± 0.15	0.12 ± 0.01	pH 5.0	0.5	2.09 ± 0.31	0.17 ± 0.01
0.9 Hq	0.5	0.322 ± 0.048	0.07 ± 0.01	0.9 Hq	0.5	0.479 ± 0.072	0.05 ± 0.01
pH 7.0	0.2	0.084 ± 0.013	0.15 ± 0.01	pH 7.0	0.2	0.099 ± 0.015	0.09 ± 0.01
pH 8.0	0.2	0.031 ± 0.005	0.09 ± 0.01				
Competition assays	assays						
DNQX-GIu °	(MH)	, (hм) ^д	A ^{DNQX·LBD} (rel.) ^b	DNQX (µll)		K _d ^{Glu} (µM)	A ^{Glu} ·LBD (rel.) ^b
0.9 Hq	0.5	0.322	0.09 ± 0.01	2.41	0.1	0.159 ± 0.024	0.54 ± 0.01
pH 7.0	0.5	0.084	0.22 ± 0.01	2.41	0.1	0.166 ± 0.025	0.61 ± 0.01
0.8 Hq	0.5	0.031	0.32 ± 0.01	2.41	0.1	0.147 ± 0.022	0.71 ± 0.01

measurement error, based on repeated measurements. This led to fitting error estimates that were <15 % for all K_d values and 1-2 % for all amplitude values. For analyzing the competition assays we set K_d^{DNOX} to the indicated values, however, taking the Analysis of the titration data shown in Fig. 2 and Fig. 3. Direct binding was evaluated with Eq. 2bc and competition assays with Eq. S2 using non-linear least square fitting. In all cases we set $K_{\rm lF}$ = 33.5 μ M. For individual data points we assumed a 2% 15 % error estimates of these values into account did do not increase the error to >15 % for K_d^{Glu} . K_d values that we determined from separate, independent measurements were within the 15 % confidence intervals, as well.

^a apparent dissociation constant from binding assays

^b amplitude relative to apo-LBD fluorescence A^{apo-LBD} d set constant for fitting $^{\circ}$ measured in the presence of 2.41 μM DNQX